Characterization of natural photonic crystals in iridescent wings of damselfly Chalcopteryx rutilans by FIB/SEM, TEM, and TOF-SIMS

David M. Carr, Ashley A. Ellsworth, Gregory L. Fisher, Wescley W. Valeriano, Juan P. Vasco, Paulo S. S. Guimarães, Rodrigo R. de Andrade, Elizabeth R. da Silva, and Wagner N. Rodrigues

---

Articles you may be interested in

Biomedical surface analysis: Evolution and future directions (Review)
Biointerphases **12**, 02C301 (2017); 10.1116/1.4982169

NanoSIMS for biological applications: Current practices and analyses
Biointerphases **13**, 03B301 (2018); 10.1116/1.4993628

Orientation and characterization of immobilized antibodies for improved immunoassays (Review)
Biointerphases **12**, 02D301 (2017); 10.1116/1.4978435

Evaluation of matrix effects on TOF-SIMS data of leu-enkephalin and 1,2-dioleoyl-sn-glycero-3-phosphocholine mixed samples
Biointerphases **13**, 03B403 (2018); 10.1116/1.5013219

Combining CXCR4-targeted and nontargeted nanoparticles for effective unassisted in vitro magnetic hyperthermia
Biointerphases **13**, 011005 (2018); 10.1116/1.5009989

Caspofungin on ARGET-ATRP grafted PHEMA polymers: Enhancement and selectivity of prevention of attachment of Candida albicans
Biointerphases **12**, 05G602 (2017); 10.1116/1.4986054

Characterization of natural photonic crystals in iridescent wings of damselfly *Chalcopteryx rutilans* by FIB/SEM, TEM, and TOF-SIMS

David M. Carr,[a] Ashley A. Ellsworth, and Gregory L. Fisher
Physical Electronics, Inc., 18725 Lake Drive East, Chanhassen, Minnesota 55317

Wescley W. Valeriano, Juan P. Vasco, and Paulo S. S. Guimarães
*Departamento de Física, ICEx, Universidade Federal de Minas Gerais, Av. Antônio Carlos 6627,
31270-901 Belo Horizonte, Minas Gerais, Brazil*

Rodrigo R. de Andrade
*Centro de Microscopia, Universidade Federal de Minas Gerais, Av. Antônio Carlos 6627,
31270-901 Belo Horizonte, Minas Gerais, Brazil*

Elizabeth R. da Silva
*Departamento de Morfologia, ICB, Universidade Federal de Minas Gerais, Av. Antônio Carlos 6627,
31270-901 Belo Horizonte, Minas Gerais, Brazil*

Wagner N. Rodrigues
*Departamento de Física, ICEx, Universidade Federal de Minas Gerais, Av. Antônio Carlos 6627,
31270-901 Belo Horizonte, Minas Gerais, Brazil*

The iridescent wings of the *Chalcopterix rutilans* damselfly (Rambur) (Odonata, Polythoridae) are investigated with focused ion beam/scanning electron microscopy, transmission electron microscopy, and time-of-flight secondary ion mass spectrometry. The electron microscopy images reveal a natural photonic crystal as the source of the varying colors. The photonic crystal has a consistent number and thickness ($\sim$195 nm) of the repeat units on the ventral side of the wing, which is consistent with the red color visible from the bottom side of the wing in all regions. The dorsal side of the wing shows strong color variations ranging from red to blue depending on the region. In the electron microscopy images, the dorsal side of the wing exhibits varied number and thicknesses of the repeat units. The repeat unit spacings for the red, yellow/green, and blue regions are approximately 195, 180, and 145 nm, respectively. Three-dimensional analysis of the natural photonic crystals by time-of-flight secondary ion mass spectrometry reveals that changes in the relative levels of Na, K, and eumelanin are responsible for the varying dielectric constant needed to generate the photonic crystal. The photonic crystal also appears to be assembled with a chemical tricomponent layer structure due to the enhancement of the $CH_6N_3^+$ species at every other interface between the high/low dielectric constant layers. *Published by the AVS.* https://doi.org/10.1116/1.5019725

I. INTRODUCTION

Many biological systems present periodic variations of the refractive index in the submicron range, which results in strong and diverse optical effects.[1–8] Since these effects are generated from physical variations instead of pigments, they are referred to as structural colors. The optical effects include bright colors and light polarization as well as angle dependent reflectance. Natural systems presenting structural colors can show different strategies for producing the optical effects such as multilayered systems, regular arrangements of scales, and tunable photonic crystals. The study of structural colors serves the dual motivation of understanding interesting natural phenomena and biomimetic inspiration to solve challenging engineering problems.

The damselfly *Chalcopteryx rutilans* (Rambur) (Odonata, Polythoridae) is an Amazonian rain forest species with brightly colored iridescent wings. The wings play an important role in their reproductive behavior.[9] *C. rutilans* has transparent anterior wings and brightly colored posterior wings, which give rise to its common name—the glitterwing. Female individual wings have a reddish color seen on both the dorsal (top) and ventral (bottom) sides of the wing. For the male, the ventral side of the wing shows a similar reddish color as that seen in the female. The dorsal side of the male wing, however, displays colors that span the visible wavelength spectrum, including red, blue, and yellow/green regions.

The first study on the origin of the colors observed in this species was performed by Valeriano,[10] who studied the optical and structural properties of the iridescent wings of *C. rutilans* damselfly. However, the chemical constitution of the multilayered wings of that damselfly has not been studied yet. Valeriano[10] hypothesized that the observed periodic layer structure involved chitin with varying levels of melanin.

Melanin is a generic term for a variety of naturally occurring polymeric pigments widely found in nature. A very general definition of melanin is "heterogeneous polymer derived by the oxidation of phenols and subsequent polymerization of intermediate phenols and their resulting

[a]Electronic mail: dcarr@phi.com

quinones."[11] The most common melanin in invertebrates is eumelanin.[12] Melanins do not have fixed compositions due to the random polymerization of the various phenol and quinone units. Strong carbon–carbon bonds linking the melanin monomer units are nonhydrolyzable and resist chemical analysis due to the insolubility of the resulting polymers.[13] Melanins are effective cation chelating agents due to the favorable energetics for them to exist in a negatively charged state.[14]

Previous time-of-flight secondary ion mass spectrometry (TOF-SIMS) analyses of eumelanin have failed to show distinct characteristic monomer ion peaks for eumelanin.[15–19] This is not surprising given the strong carbon–carbon bonds between the monomer units. The previous studies used a series of negative ion peaks as a fingerprint to indicate the presence of eumelanin.

In this work, the multilayered structure of the *C. rutilans* wing was investigated through focused ion beam (FIB)/scanning electron microscopy (SEM) and transmission electron microscopy (TEM) and correlated with chemical identification achieved by TOF-SIMS.

II. EXPERIMENT

A. FIB/SEM

The FIB/SEM experiments were conducted on a FEI Dual Beam Microscope Quanta 3D FEG (FEI Company, Hillsboro, OR). The wing was attached to the aluminum sample holder with a ribbon of conductive carbon tape. To reduce charging due to the electron beam under SEM analysis, the wing surface was carbon coated.

The FIB cross-sections were polished using a 30 keV Ga ion beam and 1 nA ion beam current. The angle of incidence of the beam was +3° (the bottom edge was exposed). The scanning line of the ion beam was moved manually toward the wing from the edge. For each polishing step, the quality of the cross-section polishing was verified by taking electron micrographs. The procedure was followed until the cross-section was judged as smooth enough to show the different layers clearly. At this point the angle of the beam was set to +5°, the current reduced to 0.1 nA, and a final polishing run was performed.

The SEM secondary electron images were taken with 2 keV beam energy, 10 mm working distance, and 35 000× magnification.

B. TEM

The wing was prepared for TEM analyses after removal of its natural wax coating by immersion in chloroform. It was immersed in a Karnovsky modified cacodylate buffered solution followed by 2% osmium tetroxide. The wing was then dehydrated and embedded in EPON resin. Thirty nanometer thick sections were prepared by ultramicrotomy with a diamond blade and analyzed on a Tecnai G2–12 Spirit BioTwin (FEI Company, Hillsboro, OR) at 80 kV.

C. TOF-SIMS

The TOF-SIMS experiments were conducted on a PHI *nanoTOF* II TOF-SIMS with Parallel Imaging MS/MS
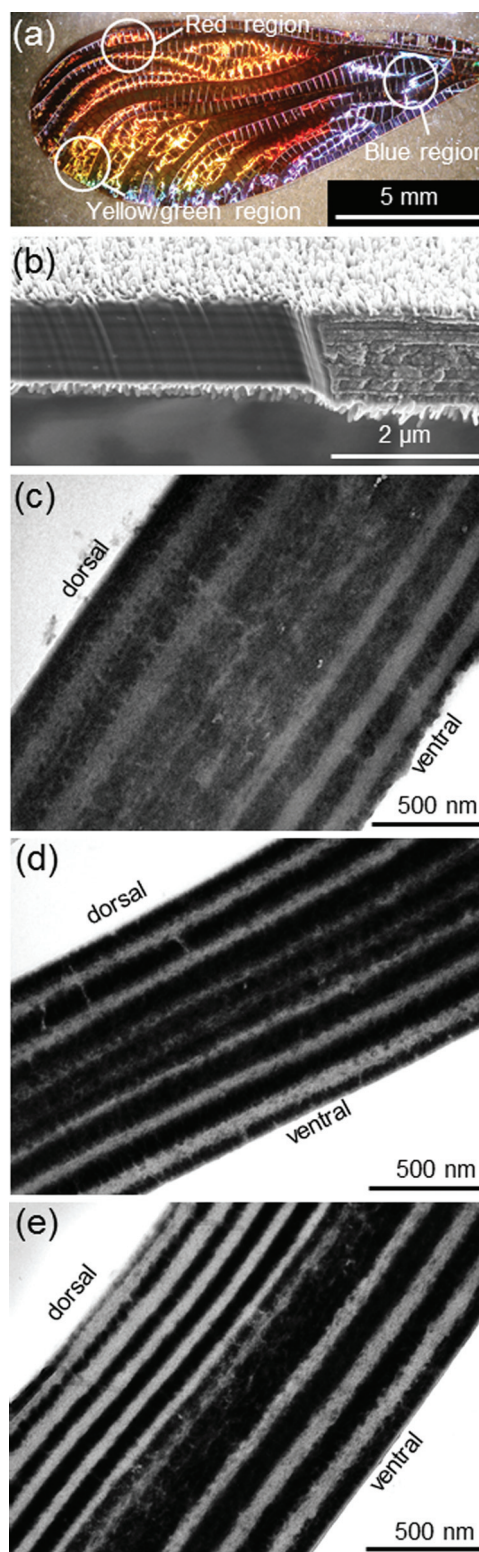

FIG. 1. (a) Optical image of male *C. rutilans* wing with representative areas where FIB cross sections were performed. (b) FIB-SEM cross section for yellow/green region. TEM cross sections for (c) red, (d) yellow/green, and (e) blue regions.

(Physical Electronics, Chanhassen, MN). A pulsed 30 kV Bi_3^+ beam was used for analysis in a 200 μm field of view. A 20 kV Ar_{2500}^+ gas cluster ion beam was used for depth profiling through the wing with a beam current of ~4 nA and an 800 × 800 μm sputter raster area. The depth profiles were acquired in a phased profile mode with each cycle consisting of 16 s of analysis (6.8×10^9 Bi_3^+/cm^2) followed by 15 s of sputtering (5.9×10^{13} Ar_{2500}^+/cm^2). The intact wings were mechanically clamped between a wide mesh stainless steel grid and a Cu/Be backing plate for analysis. No coatings or adhesives were required for analysis. Charge compensation was performed using a pulsed e-gun (~25 eV) in both polarities and low energy (~10 eV) Ar^+ ions in the positive polarity.

III. RESULTS AND DISCUSSION

A. Characterization of the physical wing structure

Figure 1(a) shows an optical image of a male damselfly wing where the circles indicate the regions of FIB cross sections and SEM analyses. SEM reveals a multilayered structure with alternating light and dark bands of varying

electronic densities in the yellow/green region of the wing [Fig. 1(b)]. The irregular features on the top and bottom of the wing are the natural wax coating. Similar banding was also present in the red and blue regions. Figures 1(c)–1(e) show the resulting TEM images for the red, yellow/green, and blue regions of the wing, respectively. In these images, the multilayered structure is more easily observed than in SEM due to the higher spatial resolution and OsO_4 staining.

The number and thickness of the alternating dark and light bands varies largely in the dorsal and ventral surfaces of the wing. The repeating unit (a light and dark band measured together) has the same pitch of 195 nm all over the ventral surface, which is consistent with its homogeneous red color. On the contrary, the dorsal side of the wing exhibits varied number and thicknesses of the repeating units accordingly to the optically visible color. The repeating unit for the red, yellow/green, and blue regions has thicknesses of approximately 195, 180, and 145 nm, respectively.

Valeriano[10] measured the spectral optical reflectance of the male wing and compared the data with the theoretical reflectance calculated through the transfer matrix method
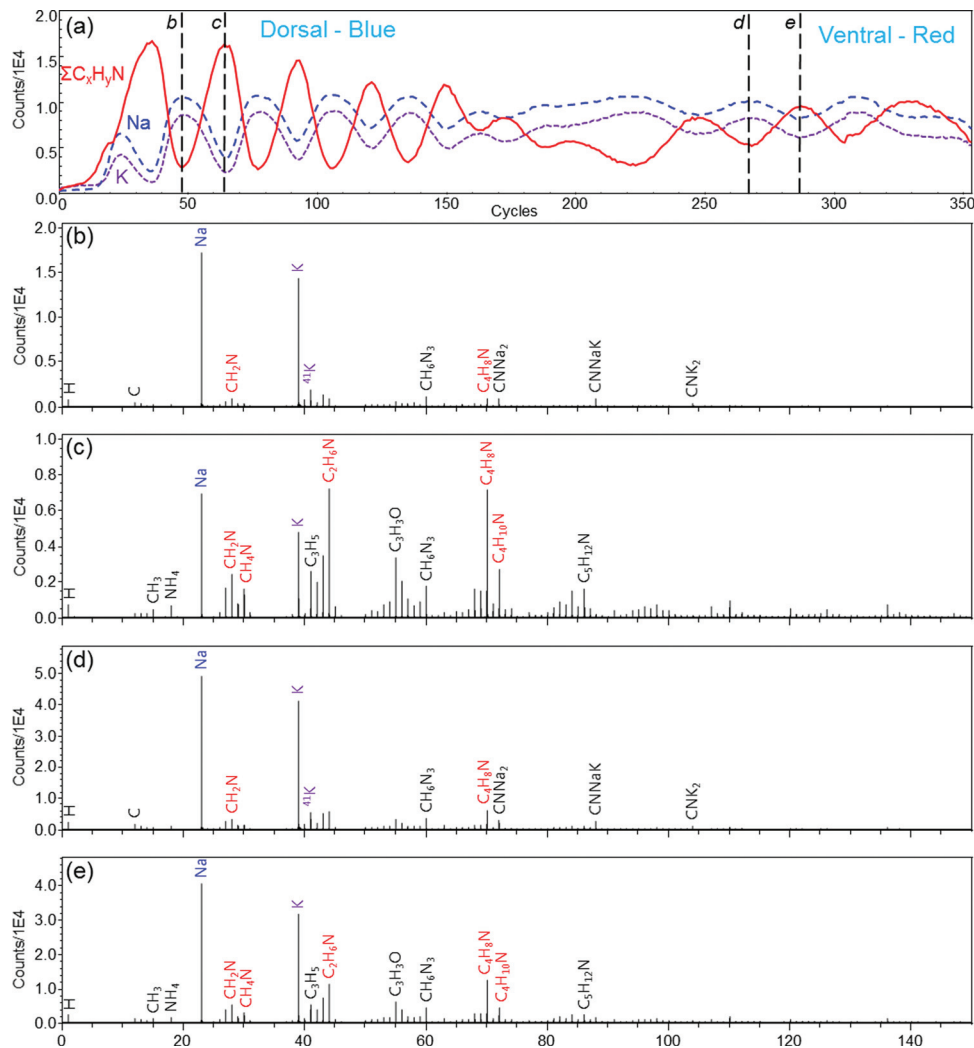

FIG. 2. (a) Positive ion TOF-SIMS depth profile for a blue region on a colored posterior wing. Extracted positive ion spectra from the dorsal portion of the wing for (b) a high Na layer and (c) a high C_xH_yN layer and from the ventral portion of the wing for (d) a high Na layer and (e) a high C_xH_yN layer.

using the structural information from the electron micros-copy images. It could be demonstrated that the layered struc-ture of the wing produces the observed colors, suggesting that the iridescent wings of the *C. rutilans* damselfly are nat-ural photonic crystals.

B. TOF-SIMS chemical analysis of wings

While the electron microscopy images were useful in the elucidation of the physical structure of the natural photonic crystals responsible for the varying colors, they were unable to give clues about the chemistry of the different layers. FTIR and Raman measurements were not able to identify any chemistry variations to explain the layered structure observed in the electron microscopy experiments due to the lack of the necessary spatial resolution. Therefore, 3D depth profiling of the wings was performed using TOF-SIMS to gain an understanding of the wing chemistry. Only ionized species are detected in TOF-SIMS. Therefore, the following data will present separate positive ion and negative ion results since they must be acquired in sequential experiments.

The positive ion depth profile from a blue region of the colored wing is shown in Fig. 2(a). The wing was analyzed from the dorsal (top) surface down into the wing. The col-ored wing profile shows periodic oscillations in ion intensi-ties that vary between the dorsal and ventral regions of the wing. The periodic oscillations are consistent with the elec-tron microscopy results. Three species are shown in the depth profile graphs: Na^+, K^+, and $\sum C_xH_yN^+$. $\sum C_xH_yN^+$ is the summation of CH_2N^+, CH_4N^+, $C_2H_4N^+$, $C_2H_6N^+$, $C_4H_8N^+$, and $C_4H_{10}N^+$. These ion species were selected for plotting due to their large variations in intensity between layers. The slow rise in signal levels at the beginnings of the profiles is due to the natural hydrocarbon wax present on the surface of the wings. For simplicity, no characteristic peaks for the wax were plotted.

In TOF-SIMS, complete mass spectra are recorded at every pixel at every sputter depth. Spectra and images can be extracted from any depth in the profile. Figures 2(b)–2(e) show the spectra extracted from two different layers in both the dorsal and ventral regions of the profile as indicated by the dashed black lines. Figure 2(b) is the extracted spectrum
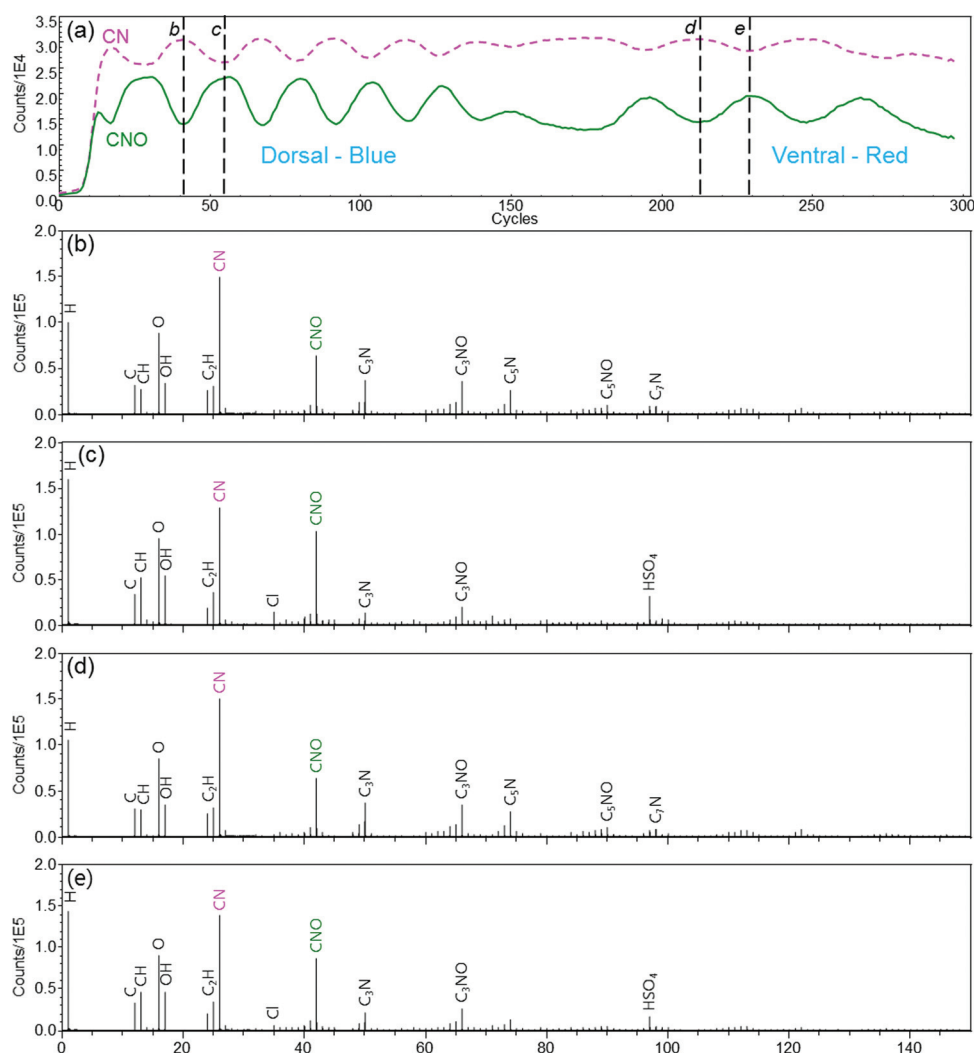

FIG. 3. Negative ion TOF-SIMS depth profile for a blue region on a colored posterior wing. Extracted negative ion spectra from the dorsal portion of the wing for (b) a high CN layer and (c) a high CNO layer and from the ventral portion of the wing for (d) a high CN layer and (e) a high CNO layer.

from a layer in the dorsal region where the relative Na^+ and K^+ signals are high and the relative $\sum C_xH_yN^+$ signal is low. For the purposes of this discussion, this will be referred to as a "high Na" layer. Figure 2(c) is the extracted spectrum from a layer in the dorsal region where the relative $\sum C_xH_yN^+$ signal is high and the relative Na^+ and K^+ signals are low and will be referred to as a "high C_xH_yN" layer. Figures 2(d) and 2(e) show similar high Na and high C_xH_yN layer spectra extracted from the ventral region in the profile.

As seen in Figs. 2(c) and 2(e), the high C_xH_yN layers have stronger relative signal level for many organic peaks when compared to the high Na layers. This is most clearly seen in the amine peaks highlighted in red that were used to generate the $\sum C_xH_yN^+$ profile. The high Na layers in Figs. 2(c) and 2(e) also have higher mass Na/K adduct peaks with CN. While the depth profiles are only shown for Na^+, K^+, and $\sum C_xH_yN^+$, the profiles show very similar periodic behavior for most of the characteristic peaks stronger in one layer compared to the other. The high Na and high C_xH_yN extracted layer spectra are consistent between the dorsal/blue and ventral/red regions of the profile. The amplitude of the oscillations decreases through the profile, which may be due to sample roughening during sputtering.

To make sure any chemistry variation detected by TOF-SIMS was truly indicative of the layer structure, the clear anterior wing of the *C. rutilans* damselfly was also analyzed as a control sample. See supplementary material for the profile and spectral data from the clear wing.[22] To summarize that data, the clear wing is substantially thinner than the colored wing, it has no periodic oscillating repeat layers, and the chemistry is similar to the colored wing, but with less enhancement of the Na and K peaks and no strong higher mass Na/K adduct peaks with CN.

The same profile experiments on colored and clear wings were performed in the negative polarity to get a more complete view of the chemistry. Similar periodic variations in chemical composition were also detected in the negative ion depth profiles as seen in Fig. 3(a) for a second blue region on the colored wing. In this polarity, strong variation in the relative CN^- and CNO^- signals are clearly observed between layers. Figures 3(b)–3(e) again show the spectra extracted from two different layers in both the dorsal and ventral regions of the profile as indicated by the dashed black lines. Figure 3(b) is the extracted spectrum from a layer in the dorsal region where the relative CN^- signal was high and the relative CNO^- signal was low. For the purposes of this discussion, this will be referred to as a "high CN" layer. Figure 3(c) is the extracted spectrum from a layer in the dorsal region where the relative CNO^- signal was high and the relative CN^- signal was low and will be referred to as a "high CNO" layer. Figures 3(d) and 3(e) show similar high CN and high CNO layer spectra extracted from the ventral region in the profile. The high CN layer corresponds with the high Na layer seen in the positive ion depth profile, while the high CNO layer corresponds with the high C_xH_yN layer from the positive depth profile. Although the high Na/CN layers have elevated Na^+/K^+ levels, the high C_xH_yN/CNO

layers have elevated relative signal levels for Cl^- and HSO_4^- compared to the high CN layer. Therefore, the elevated Na^+/K^+ does not appear to be present as a simple ionic salt.

The negative ion results of the clear wing are also available in the supplementary material. The data are consistent with the positive ion results and show less enhancement of the CN peak when compared to the colored wing.

Since complete mass spectra are recorded at every pixel at every depth, 3D images can be generated in addition to spectra and 2D images. Figure 4(a) shows the 3D isosurface image for Na^+ and $\sum C_xH_yN$. Figure 4(b) shows the 3D isosurface image for CN^-, CNO^-, and m/z 423^-. The peak present at m/z 423^- was a characteristic high mass peak on the
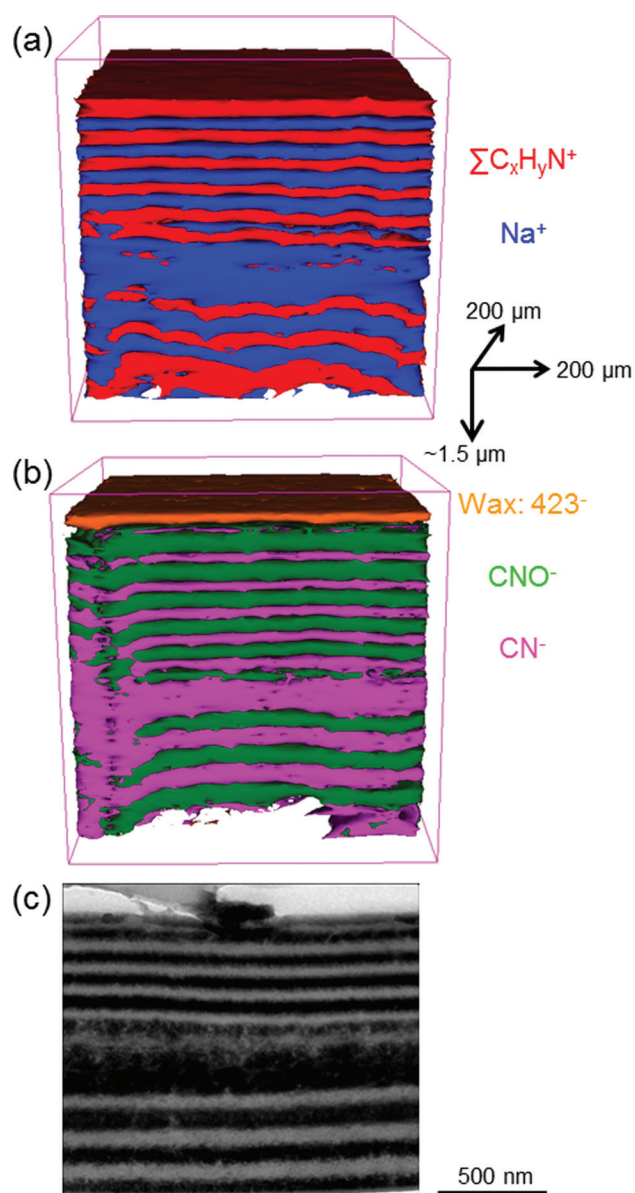

FIG. 4. (a) 3D isosurface image reconstructed from the positive ion TOF-SIMS depth profile of a blue region. (b) 3D isosurface image reconstructed from the negative ion TOF-SIMS depth profile of a blue region. (c) TEM image for a similar blue area.

surface which can be attributed to the surface hydrocarbon wax. Figure 4(c) shows the TEM image obtained from the cross section of a blue region of the wing, and indicates that the layered structure observed in both TOF-SIMS 3D ion imaging and TEM imaging correlate strongly. One difference worth noting, however, is the length scales. The scale bar marker in the TEM image is 500 nm. The x-y dimensions in the TOF-SIMS 3D images are 200×200 μm, while the z-dimension is ~1.5 μm. If the z-dimension was similarly scaled, the layer structure would be too compacted to see. This data, stretched in the z-dimension, show that the wing layers have uniform thicknesses over large distances (>200 μm).

C. Photonic crystal chemistry—The role of melanin

The TOF-SIMS data in Sec. III B clearly correlated with the physical structure observed by FIB/SEM and TEM. To investigate the hypothesis by Valeriano[10] that varying levels of melanin are responsible for the photonic crystal layers, a reference sample of commercially available synthetic melanin (Sigma-Aldrich) was analyzed. Although the catalog lists it simply as melanin, this is synthetic eumelanin which is the most common melanin found in insects. Figure 5(a) shows the negative ion spectrum from the synthetic eumelanin while Figs. 5(b) and 5(c) show the high CN layer and the high CNO layer spectra extracted from the dorsal portion of the blue colored wing region. Figure 5 shows that there is a very good agreement between the synthetic eumelanin spectrum and the high CN spectrum. The prominent peaks correlate well with the peaks used to fingerprint eumelanin in the literature.[15–19] The eumelanin fingerprint peaks are also present in the CNO layer, but at lower relative levels.

Other factors also correlate well with the presence of eumelanin in the high CN layer. The high CN layer has elevated Na^+/K^+ levels. This is consistent with the fact that eumelanin is an effective cation chelating agent. Additionally, osmium tetroxide is routinely used in electron microscopy as a contrast enhancing agent due to its affinity to unsaturated bonds and strong electron scattering.[20] In the TEM images, the dark areas correspond to the high Na/CN layers. The darkness is likely due to increased electron scattering by Os along with increased electron scattering from the higher Na and K levels. Eumelanin is a highly unsaturated polymer that is osmiophilic. The TOF-SIMS spectra do not show strong peaks with unsaturated bonds, but the relative H signal level is lower in the high Na/CN layers, which is consistent with higher degrees of unsaturation. As mentioned in Sec. I, the strong C–C bonds between the monomer units in eumelanin create highly fragmented spectra with no clear molecular ion monomer peaks, making it more difficult to clearly identify unsaturated fragments in the TOF-SIMS spectra.

Therefore, these results taken together indicate that changes in the relative level of Na, K, and eumelanin are responsible for the chemical variation in the natural photonic crystal layers.

D. Importance of interfaces

As mentioned earlier, the depth profiles for the colored wing show very similar periodic behavior for most of the characteristic peaks stronger in one layer compared to the other layer. The notable exception was the $CH_6N_3^+$ ion. Figure 6(a) shows the depth profiles of $CH_6N_3^+$, Na^+, and $\sum C_xH_yN^+$ for the colored wing blue region. The $CH_6N_3^+$ curve has been multiplied by 4 to make the profile features easier to see on the same axes. This figure shows that the
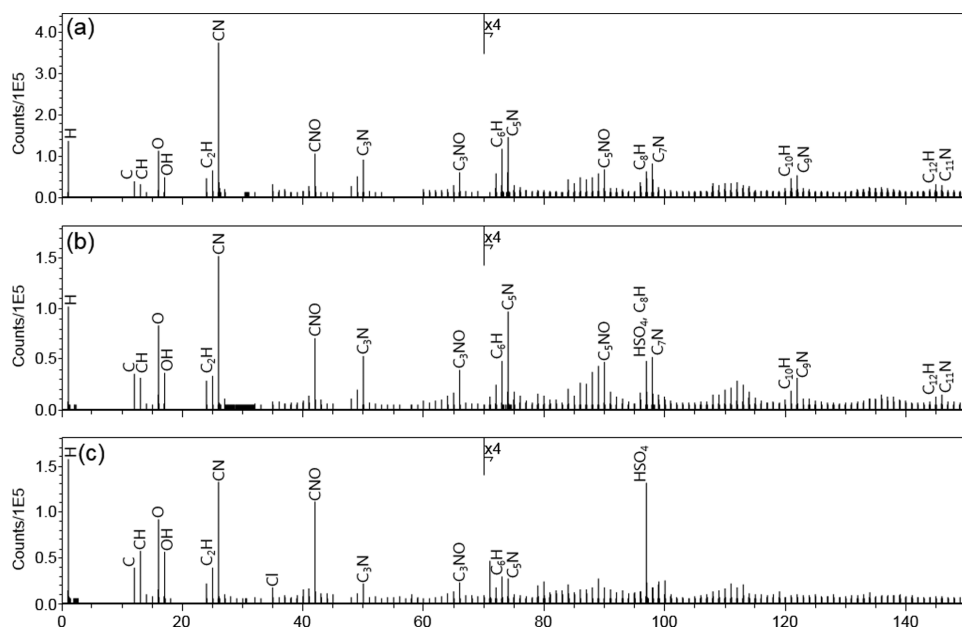

Fig. 5. Negative ion TOF-SIMS spectra from (a) the synthetic eumelanin compared to (b) a high CN layer and (c) a high CNO layer extracted from the dorsal portion of the colored wing blue region.
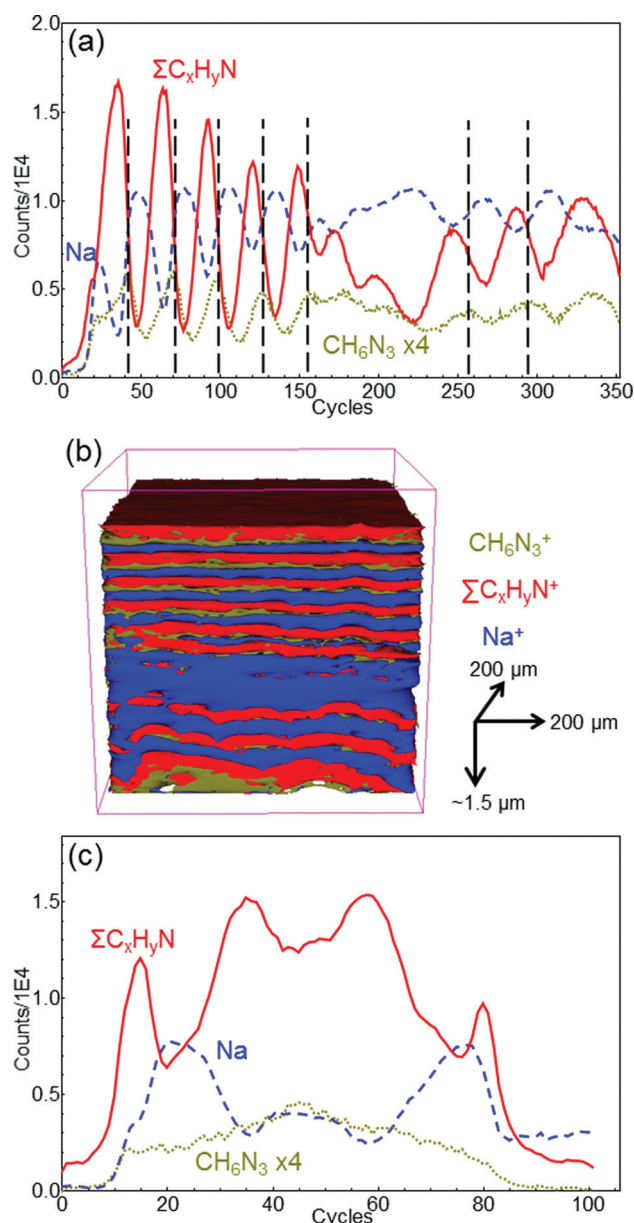
FIG. 6. (a) Positive ion TOF-SIMS depth profiles for a blue region on a colored posterior wing of *C. rutilans* damselfly and (b) 3D isosurface image reconstructed from the positive ion TOF-SIMS depth profile of a blue region with $CH_6N_3^+$ signal intensity maximum at every other interface. (c) Corresponding positive ion TOF-SIMS depth profiles for a clear anterior wing of *C. rutilans* damselfly where there are no $CH_6N_3^+$ signal intensity maximums at interfaces.

intensity of the $CH_6N_3^+$ species has a maximum at every other interface between the high Na and high C_xH_yN layers. This behavior is also visible in the 3D image in Fig. 6(b). This suggests that the structure of the blue region of the wing which appeared as a bilayer structure in the electron microscopy images is actually a tricomponent chemical structure as shown by TOF-SIMS. Figure 6(c) shows the corresponding depth profiles of $CH_6N_3^+$, Na^+, and $\sum C_xH_yN^+$ for the clear wing. The $CH_6N_3^+$ curve has again been multiplied by 4 to make the profile features easier to see on the same axes. In the clear wing, this $CH_6N_3^+$ species does not

peak at the interfaces. This is consistent with the lack of a well-defined periodic repeating structure in the clear wing.

Mass resolutions on these flexible wings were greater than 3000 throughout the profiles. The peak assignment of $CH_6N_3^+$ is the best match to the data both in terms of peak position and isotopic matching of the surrounding peaks. Based on the peak exact mass (60.05), the peak is definitely organic and not a Na or K adduct peak arising as an interfacial artifact.

While a trilayered structure was not expected, it may provide clues about the thermodynamics of layer growth during the formation of the wing. It is well known in semiconductor heteroepitaxy that given two semiconductors A and B, the formation of an ABAB… superlattice is challenging due to the fact that if A wets B for smooth two-dimensional growth, then B will not wet A and will start growing in a three-dimensional fashion.[21] One method to overcome this is through the use of a surfactant to change the surface energy of B to aid in the two-dimensional growth of A onto B. Extending this knowledge to these findings, the $CH_6N_3^+$ may be present between layers because it could serve as a wetting layer to aid in the growth of the multilayer natural photonic crystal. It could also help with adhesion between the layers. Further investigation could reveal if the $CH_6N_3^+$ ion is a fragment of a larger molecule present at the interface.

IV. SUMMARY AND CONCLUSIONS

The combination of FIB/SEM/TEM for structural characterization and TOF-SIMS for chemical characterization showed that the multilayered structure of the *C. rutilans* iridescent wings contains oscillating levels of Na, K, and eumelanin that could be responsible for the varying dielectric constant needed to generate a natural photonic crystal. The repeating unit (dark and light bands) appears to be in fact a tricomponent assembly as suggested by the enhancement of the $CH_6N_3^+$ species at every interface between the high/low dielectric constant layers.

Future experiments will include TOF-SIMS analysis of the red and yellow/green wing regions to confirm that the changes in color are only due to the number and thickness of the repeating units and not due to some additional chemistry differences. A control sample of a uniformly pigmented wing could also be instructive.

[1]J. Teyssier, S. V. Saenko, D. van der Marel, and M. C. Milinkovitch, Nat. Commun. **6**, 6368 (2015).
[2]M. R. Nixon, A. G. Orr, and P. Vukusic, Opt. Express **21**, 1479 (2013).
[3]D. G. Stavenga, H. L. Leertouwer, T. Hariyama, H. A. De Raedt, and B. D. Wilts, PLoS One **7**, e49743 (2012).

[4]P. Vukusic and D. G. Stavenga, J. R. Soc. Interface **6**, S133 (2009).

[5]A. R. Parker and N. Martini, Opt. Laser Technol. **38**, 315 (2006).

[6]D. J. Brink and N. G. van der Berg, J. Phys. D: Appl. Phys. **37**, 813 (2004).

[7]J. Zi, X. Yu, Y. Li, X. Hu, C. Xu, X. Wang, X. Liu, and R. Fu, Proc. Natl. Acad. Sci. U. S. A. **100**, 12576 (2003).

[8]M. F. Land, Prog. Biophys. Mol. Biol. **24**, 75 (1972).

[9]D. C. Resende and P. de Marco, Jr., Rev. Bras. Entomol. **54**, 436 (2010).

[10]W. W. Valeriano, "Cores estruturais da asa da libélula *Chalcopteryx rutilans*," Masters dissertation (UFMG, 2015).

[11]F. Solano, New J. Sci. **2014**, 498276.

[12]A. J. Garcia, C. Polidori, and J. L. Nieves-Aldrey, Arthropod Struct. Dev. **45**, 311 (2016).

[13]J. D. Simon and S. Ito, Pigm. Cell Res. **17**, 423 (2004).

[14]T. Sarna, J. S. Hyde, and H. M. Swartz, Science **192**, 1132 (1976).

[15]J. Lindgren, P. Uvdal, P. Sjövall, D. E. Nilsson, A. Engdahl, B. P. Schultz, and V. Thiel, Nat. Commun. **3**, 824 (2012).

[16]J. Lindgren *et al.*, Nature **506**, 484 (2014).

[17]M. E. McNamara, B. E. van Dongen, N. P. Lockyer, I. D. Bull, and P. J. Orr, Palaeontology **59**, 337 (2016).

[18]C. C. Labandeira *et al.*, Proc. R. Soc. B **283**, 20152893 (2016).

[19]J. A. Gren *et al.*, Palaeontology **60**, 73 (2017).

[20]J. J. Bozzola and D. L. Russell, *Electron Microscopy: Principles and Techniques for Biologists*, 2nd ed. (Jones and Bartlett, Sudbury, MA, 1999).

[21]C. J. Palmstrøm, Annu. Rev. Mater. Sci. **25**, 389 (1995).

[22]See supplementary material at https://doi.org/10.1116/1.5019725 for positive and negative polarity profiles and spectra from a clear wing.